

Compact hidden charmed pentaquark states and QCD isomers

Cheng-Rong Deng^{a,b*}

^a*School of Physical Science and Technology, Southwest University, Chongqing 400715, China and*

^b*School of Physics and Center of High Energy Physics, Peking University, Beijing 100871, China*

We make an exhaustive investigation on the pentaquark states $qqq\bar{c}$ ($q = u, d$ and s) and discuss the effect of color structures in a multiquark color flux-tube model. We exhibit a novel picture of the structure and properties of the states P_c and P_{cs} observed by the LHCb Collaboration. We can describe the states as the compact pentaquark states in the model. The spin-parity of the group of $P_c(4312)^+$ and $P_c(4337)^+$ is $\frac{1}{2}^-$ while that of the group of $P_c(4380)^+$, $P_c(4440)^+$ and $P_c(4457)^+$ is $\frac{3}{2}^-$. Their structures are pentagon, diquark, pentagon, diquark, and octet, respectively. The members in each group can be analogically called QCD isomers because of their the same spin-parity and quark content but different color structures. The singlet $P_{cs}(4459)^0$ has pentagon structure and spin-parity of $\frac{1}{2}^-$. In addition, we also predict the P_{cs} , P_{css} and P_{csss} families in the model. The five-body confinement potential based on the color flux-tube picture, which is a collective degree of freedom and induces QCD isomer phenomenon, plays an important role in the formation of the compact states.

I. INTRODUCTION

Conventional baryons are composed of three valence quarks in the constituent quark models. Exploring exotic baryons consisting of four valence quarks and one valence antiquark, called pentaquark states, has been one of the most significant research topics in the hadron physics since the birth of the quark model [1]. The existence of fully-light pentaquark states is apt to be negative so far [2]. In the charm sector, there were many predictions on the hidden charmed pentaquark states [3–7]. Recently, the LHCb Collaboration reported the hidden charmed pentaquark states $P_c(4380)^+$, $P_c(4312)^+$, $P_c(4440)^+$, $P_c(4457)^+$, $P_{cs}(4459)^0$, and $P_c(4337)^+$ in the $J/\psi p$ or $J/\psi \Lambda$ invariant mass spectrum [8–11]. Their masses, widths and minimal valence quark contents are presented in Table I. However, the reliable information about their spin-parity has been unavailable until now.

Systematical study on their nature and structure can improve our understanding of the non-perturbative behaviors of the strong interaction. Therefore, a lot of theoretical explanations have been devoted to their properties, such as hadron molecular states [12–16], compact

pentaquark states [17–22], kinematical effects [23, 24], and hadrocharmonium [25, 26], virtual states [27], and double triangle cusps [28], within different theoretical frameworks. The latest reviews can be found in Refs. [29], in which the molecular state is overwhelming because of the proximity of their masses to the baryon-meson thresholds. Even so, there were no conclusive consensus on their properties, especially for the states $P_c(4440)^+$ and $P_c(4457)^+$ because of their ambiguous spin [30].

The color structures of mesons and baryons are unique while the multi-quark states have abundant color structures [31, 32]. The effect of various color structures, which is absent in the mesons and baryons, may raise in the multiquark states. The states P_c and P_{cs} provide a good platform to explore the effect. In the previous work [18], we studied the state $P_c(4380)^+$ and proposed a novel color flux-tube structure, a pentagon state, for the pentaquark states in the multiquark color flux-tube model. In the present work, we prepare to make a systematical investigation on the hidden-charm pentaquark states in the model. We anticipate to exhibit new insights into the properties and structures of the P_c and P_{cs} states from the perspective of the phenomenological model. We also hope that this work can improve the understanding of the mechanism of the low-energy strong interactions.

This paper is organized as follows. After the introduction, Sec. II gives the descriptions of the model. Sec. III presents the wave functions of the hidden charm pentaquark states. Sec. IV shows the numerical results and discussions. The last section lists a brief summary.

II. MULTIQUARK COLOR FLUX-TUBE MODEL (MCFTM)

Lattice QCD investigations on mesons and baryons revealed their internal color structures [31], see FIG. 1. The quark and antiquark in mesons are linked with a three-

TABLE I: The states P_c and P_{cs} .

State	Mass (MeV)	Width (MeV)	Content
$P_c(4380)^+$ [8]	$4380 \pm 8 \pm 29$	$215 \pm 18 \pm 86$	$uudc\bar{c}$
$P_c(4312)^+$ [9]	$4311.9 \pm 0.7 \begin{smallmatrix} +6.8 \\ -0.6 \end{smallmatrix}$	$9.8 \pm 2.7 \begin{smallmatrix} +3.7 \\ -4.5 \end{smallmatrix}$	$uudc\bar{c}$
$P_c(4440)^+$ [9]	$4440.3 \pm 1.3 \begin{smallmatrix} +4.1 \\ -4.7 \end{smallmatrix}$	$20.6 \pm 4.9 \begin{smallmatrix} +8.7 \\ -10.1 \end{smallmatrix}$	$uudc\bar{c}$
$P_c(4457)^+$ [9]	$4457.3 \pm 0.6 \begin{smallmatrix} +4.1 \\ -1.7 \end{smallmatrix}$	$6.4 \pm 2.0 \begin{smallmatrix} +5.7 \\ -1.9 \end{smallmatrix}$	$uudc\bar{c}$
$P_{cs}(4459)^0$ [10]	$4458.8 \pm 2.9 \begin{smallmatrix} +4.7 \\ -1.1 \end{smallmatrix}$	$17.3 \pm 6.5 \begin{smallmatrix} +8.0 \\ -5.7 \end{smallmatrix}$	$udsc\bar{c}$
$P_c(4337)^+$ [11]	$4337 \begin{smallmatrix} +7 & +2 \\ -4 & -2 \end{smallmatrix}$	$29 \begin{smallmatrix} +26 & +14 \\ -12 & -14 \end{smallmatrix}$	$uudc\bar{c}$

*crdeng@swu.edu.cn

dimensional color flux tube. Three quarks in baryons are connected by a Y-shape flux-tube, in which \mathbf{y}_0 denotes a junction where three color flux tubes meet.

The hidden charmed pentaquark states have four possible color flux-tube structures [18], (1) meson-baryon molecular state (molecule), (2) diquark-diquark-antiquark state (diquark), (3) color octet state (octet), and (4) pentagonal state (pentagon), which are shown in FIG. 2. The corresponding positions of quarks and antiquark are denoted as $\mathbf{r}_1, \mathbf{r}_2, \mathbf{r}_3, \mathbf{r}_4$, and \mathbf{r}_5 , \mathbf{y}_i represents the i -th Y-shape junction. In some extent, color flux-tube is similar to chemical bond in QED. The QED isomers have same atom constituents but different chemical bond structures. Analogously, we can call such different structures QCD isomers.

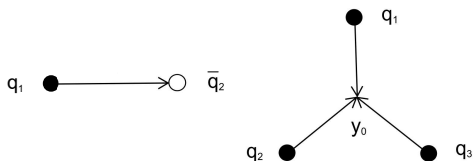


FIG. 1: Meson and baryon states.

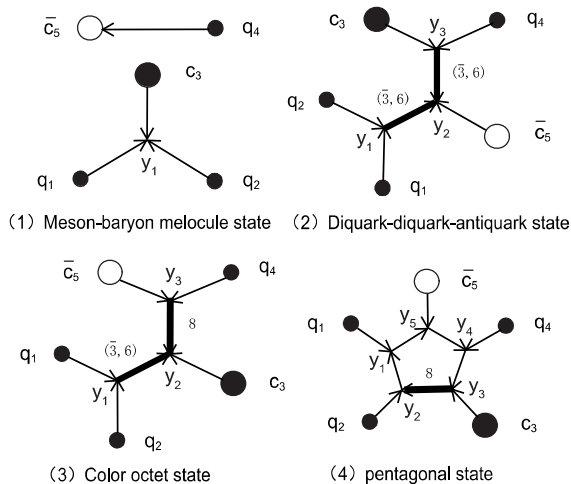


FIG. 2: Hidden charm pentaquark states.

A thin line only stands for a $\mathbf{3}$ - or $\bar{\mathbf{3}}$ -dimension color flux-tube while a thick line represents a $\mathbf{3}$ -, $\bar{\mathbf{3}}$ -, $\mathbf{6}$ -, $\bar{\mathbf{6}}$ - or $\mathbf{8}$ -dimension color flux-tube. The arrow represents the color coupling direction. Two color flux tubes meet at a Y-shape junction along with the direction of the arrows, where the coupling of two colors carried by the color flux tubes into another color carried by the third color flux tube starting from the Y-shape junction, such as the three color flux tubes $q_1\mathbf{y}_1, q_2\mathbf{y}_1$ and $\mathbf{y}_1\mathbf{y}_2$ in FIG. 2 (2) and (3), $\mathbf{3} \otimes \mathbf{3} = \bar{\mathbf{3}} \oplus \mathbf{6}$. Three color flux tubes meet a Y-shape junction along with the direction of the arrow, such as $\mathbf{y}_1\mathbf{y}_2, \mathbf{y}_3\mathbf{y}_2$ and $\bar{c}_5\mathbf{y}_2$ in the diquark structure, where three colors can couple into a color singlet.

In this way, the connection between the color flux-tube structure and the construction of the color wave function can be established clearly.

The construction of the color wave functions, no matter baryons, the pentaquark states with diquark or octet configurations, is based on the degrees of quark freedom. In another word, its starting point is always the color coupling of quark-quark or quark-antiquark in one Y-shape color flux-tube, such as q_1 - q_2 in FIG. 2 (2) or q_4 - \bar{c}_5 in FIG. 2 (3). However, none of quark-quark or quark-antiquark is in one Y-shape color flux-tube in FIG. 2 (4). Any two quarks are connected by two or more Y-shape color flux-tubes. Therefore, how to establish its color wave functions is an open question in the quark level. Even so, this ringlike structure does not violate QCD and it can form an overall color singlet. Richard also explored similar ringlike structure of hexaquark states in the string model [33]. In the present work, we first apply the wave function of the diquark structure to estimate the energy of the pentagon structure approximately.

The MCFTM has been established on the basis of the traditional quark models and lattice QCD color flux-tube picture [18, 34]. Comparing with the traditional constituent quark models, the MCFTM merely modify the sum of two-body confinement potential in the traditional models to a multi-body quadratic one. Relative to the lattice QCD, we replace the linear potential with the quadratic one. For the ground hadron states, their sizes are generally less than or around 1 fm, in which the difference between the quadratic potential and the linear one is not obvious. The difference can be further diluted by the adjustable stiffnesses of color flux-tube. The replacement is therefore reasonable in the ground states. Note that the replacement in the excited states needs to be addressed with great caution because they are spatially more extended (>1 fm). In addition, the quadratic confinement potential can greatly simplify the numerical calculation in the dynamical investigation on the multiquark states.

In the MCFTM, the two-body quadratic confinement potential for mesons can be written as

$$V_{min}^{con}(2) = k(\mathbf{r}_1 - \mathbf{r}_2)^2, \quad (1)$$

where k is the stiffnesses of a three-dimension color flux-tube. The three-body quadratic confinement potential for baryons can be written as

$$V^{con}(3) = k \sum_{i=1}^3 (\mathbf{r}_i - \mathbf{y}_0)^2 \quad (2)$$

We can determine the junction \mathbf{y}_0 of the Y-shape structure by taking the variation on the three-body quadratic confinement potential,

$$\mathbf{y}_0 = \frac{\mathbf{r}_1 + \mathbf{r}_2 + \mathbf{r}_3}{3}. \quad (3)$$

Then we can arrive at the minimum of the confinement

potential for baryons,

$$V_{min}^{con}(3) = k \left(\left(\frac{\mathbf{r}_1 - \mathbf{r}_2}{\sqrt{2}} \right)^2 + \left(\frac{2\mathbf{r}_3 - \mathbf{r}_1 - \mathbf{r}_2}{\sqrt{6}} \right)^2 \right). \quad (4)$$

According to the color flux-tube structures of the hidden charmed pentaquark states in FIG. 2, the confinement potential of the i -th color structure V_i^{con} (5) reads

$$V_1^{con}(5) = k \sum_{i=1}^3 (\mathbf{r}_i - \mathbf{y}_1)^2 + k(\mathbf{r}_4 - \mathbf{r}_5)^2, \quad (5)$$

$$V_2^{con}(5) = k \sum_{i=1}^2 (\mathbf{r}_i - \mathbf{y}_1)^2 + k \sum_{i=3}^4 (\mathbf{r}_i - \mathbf{y}_3)^2 + k \sum_{i=1,3} (\mathbf{y}_i - \mathbf{y}_2)^2 + k(\mathbf{r}_5 - \mathbf{y}_2)^2, \quad (6)$$

$$V_3^{con}(5) = k \sum_{i=1}^2 (\mathbf{r}_i - \mathbf{y}_1)^2 + k \sum_{i=4}^5 (\mathbf{r}_i - \mathbf{y}_3)^2 + k((\mathbf{y}_1 - \mathbf{y}_2)^2 + \kappa_8(\mathbf{y}_2 - \mathbf{y}_3)^2 + (\mathbf{r}_5 - \mathbf{y}_2)^2), \quad (7)$$

$$V_4^{con}(5) = k \sum_{i=2,5} (\mathbf{y}_i - \mathbf{y}_1)^2 + k \sum_{i=3,5} (\mathbf{y}_i - \mathbf{y}_4)^2 + k \sum_{i=1}^5 (\mathbf{r}_i - \mathbf{y}_i)^2 + \kappa_8 k(\mathbf{y}_2 - \mathbf{y}_3)^2 \quad (8)$$

where $\kappa_d k$ is the stiffness of the d -dimension color flux-tube, $\kappa_d = \frac{C_d}{C_3}$ [35]. C_d is the eigenvalue of the Casimir operator associated with the $SU(3)$ color representation d at either end of the color flux-tube.

We can obtain the junctions \mathbf{y}_i by taking the variation on each five-body quadratic confinement potential.

Then, we achieve the eigenvectors ξ_i , χ_i , ζ_i and η_i and their corresponding eigenvalues by diagonalizing the confinement potential matrixes. The eigenvectors are in fact the normal modes of the five-body quadratic confinement potentials, which read

$$\begin{pmatrix} \xi_1 \\ \xi_2 \\ \xi_3 \\ \xi_4 \\ \xi_5 \end{pmatrix} = \begin{pmatrix} \frac{1}{\sqrt{2}} & \frac{-1}{\sqrt{2}} & 0 & 0 & 0 \\ 0 & 0 & \frac{-1}{\sqrt{2}} & \frac{1}{\sqrt{2}} & 0 \\ \frac{1}{\sqrt{6}} & \frac{1}{\sqrt{6}} & \frac{-2}{\sqrt{6}} & 0 & 0 \\ \frac{\sqrt{2}}{\sqrt{15}} & \frac{\sqrt{2}}{\sqrt{15}} & \frac{\sqrt{2}}{\sqrt{15}} & \frac{-\sqrt{3}}{\sqrt{10}} & \frac{-\sqrt{3}}{\sqrt{10}} \\ \frac{1}{\sqrt{5}} & \frac{1}{\sqrt{5}} & \frac{1}{\sqrt{5}} & \frac{1}{\sqrt{5}} & \frac{1}{\sqrt{5}} \end{pmatrix} \begin{pmatrix} \mathbf{r}_1 \\ \mathbf{r}_2 \\ \mathbf{r}_3 \\ \mathbf{r}_4 \\ \mathbf{r}_5 \end{pmatrix}, \quad \begin{pmatrix} \chi_1 \\ \chi_2 \\ \chi_3 \\ \chi_4 \\ \chi_5 \end{pmatrix} = \begin{pmatrix} \frac{1}{\sqrt{2}} & \frac{-1}{\sqrt{2}} & 0 & 0 & 0 \\ 0 & 0 & \frac{-1}{\sqrt{2}} & \frac{1}{\sqrt{2}} & 0 \\ \frac{1}{\sqrt{4}} & \frac{1}{\sqrt{4}} & \frac{-1}{\sqrt{4}} & \frac{-1}{\sqrt{4}} & 0 \\ \frac{1}{\sqrt{20}} & \frac{1}{\sqrt{20}} & \frac{1}{\sqrt{20}} & \frac{1}{\sqrt{20}} & \frac{-4}{\sqrt{20}} \\ \frac{1}{\sqrt{5}} & \frac{1}{\sqrt{5}} & \frac{1}{\sqrt{5}} & \frac{1}{\sqrt{5}} & \frac{1}{\sqrt{5}} \end{pmatrix} \begin{pmatrix} \mathbf{r}_1 \\ \mathbf{r}_2 \\ \mathbf{r}_3 \\ \mathbf{r}_4 \\ \mathbf{r}_5 \end{pmatrix}, \quad (9)$$

$$\begin{pmatrix} \zeta_1 \\ \zeta_2 \\ \zeta_3 \\ \zeta_4 \\ \zeta_5 \end{pmatrix} = \begin{pmatrix} \frac{1}{\sqrt{2}} & \frac{-1}{\sqrt{2}} & 0 & 0 & 0 \\ 0 & 0 & \frac{-1}{\sqrt{2}} & \frac{1}{\sqrt{2}} & 0 \\ \frac{-17+\sqrt{241}}{2\sqrt{482-28\sqrt{241}}} & \frac{-17+\sqrt{241}}{2\sqrt{482-28\sqrt{241}}} & \frac{11-\sqrt{241}}{2\sqrt{482-28\sqrt{241}}} & \frac{11-\sqrt{241}}{2\sqrt{482-28\sqrt{241}}} & \frac{6}{\sqrt{482-28\sqrt{241}}} \\ \frac{-17-\sqrt{241}}{2\sqrt{482+28\sqrt{241}}} & \frac{-17-\sqrt{241}}{2\sqrt{482+28\sqrt{241}}} & \frac{11+\sqrt{241}}{2\sqrt{482+28\sqrt{241}}} & \frac{11+\sqrt{241}}{2\sqrt{482+28\sqrt{241}}} & \frac{6}{\sqrt{482+28\sqrt{241}}} \\ \frac{1}{\sqrt{5}} & \frac{1}{\sqrt{5}} & \frac{1}{\sqrt{5}} & \frac{1}{\sqrt{5}} & \frac{1}{\sqrt{5}} \end{pmatrix} \begin{pmatrix} \mathbf{r}_1 \\ \mathbf{r}_2 \\ \mathbf{r}_3 \\ \mathbf{r}_4 \\ \mathbf{r}_5 \end{pmatrix}, \quad (10)$$

$$\begin{pmatrix} \eta_1 \\ \eta_2 \\ \eta_3 \\ \eta_4 \\ \eta_5 \end{pmatrix} = \begin{pmatrix} \frac{-3-\sqrt{5}}{5\sqrt{2+\sqrt{10}}} & \frac{-3-\sqrt{5}}{5\sqrt{2+\sqrt{10}}} & \frac{-3-\sqrt{5}}{5\sqrt{2+\sqrt{10}}} & \frac{-3-\sqrt{5}}{5\sqrt{2+\sqrt{10}}} & \frac{\sqrt{2}}{\sqrt{5}} \\ \frac{3-\sqrt{5}}{5\sqrt{2-\sqrt{10}}} & \frac{2}{5\sqrt{2-\sqrt{10}}} & \frac{2}{5\sqrt{2-\sqrt{10}}} & \frac{3-\sqrt{5}}{5\sqrt{2-\sqrt{10}}} & \frac{-\sqrt{2}}{\sqrt{5}} \\ \frac{-1}{2\sqrt{5+2\sqrt{5}}} & \frac{2+\sqrt{5}}{2\sqrt{5+2\sqrt{5}}} & \frac{-2-\sqrt{5}}{2\sqrt{5+2\sqrt{5}}} & \frac{1}{2\sqrt{5+2\sqrt{5}}} & 0 \\ \frac{-1}{2\sqrt{5-2\sqrt{5}}} & \frac{2-\sqrt{5}}{2\sqrt{5-2\sqrt{5}}} & \frac{-2+\sqrt{5}}{2\sqrt{5-2\sqrt{5}}} & \frac{1}{2\sqrt{5-2\sqrt{5}}} & 0 \\ \frac{1}{\sqrt{5}} & \frac{1}{\sqrt{5}} & \frac{1}{\sqrt{5}} & \frac{1}{\sqrt{5}} & \frac{1}{\sqrt{5}} \end{pmatrix} \begin{pmatrix} \mathbf{r}_1 \\ \mathbf{r}_2 \\ \mathbf{r}_3 \\ \mathbf{r}_4 \\ \mathbf{r}_5 \end{pmatrix}. \quad (11)$$

Finally, we simplify the minimums of those quadratic confinement potentials into the sum of several independent harmonic oscillators,

$$V_{1min}^{con}(5) = k(\xi_1^2 + \xi_2^2 + \xi_3^2), \quad (12)$$

$$V_{2min}^{con}(5) = k(\chi_1^2 + \chi_2^2 + \frac{1}{3}\chi_3^2 + \frac{5}{7}\chi_4^2), \quad (13)$$

$$V_{3min}^{con}(5) = k\left(\zeta_1^2 + \zeta_2^2 + \frac{46+\sqrt{241}}{75}\zeta_3^2 + \frac{46-\sqrt{241}}{75}\zeta_4^2\right), \quad (14)$$

$$V_{4min}^{con}(5) = k\left(\frac{15+\sqrt{5}}{22}(\eta_1^2 + \eta_3^2) + \frac{15-\sqrt{5}}{22}(\eta_2^2 + \eta_4^2)\right). \quad (15)$$

The perturbative effect of QCD can be described by the one-gluon-exchange (OGE) interaction. From the non-relativistic reduction of the OGE diagram in QCD for point-like quarks one gets

$$V_{ij}^{oge} = \frac{\alpha_s}{4} \boldsymbol{\lambda}_i^c \cdot \boldsymbol{\lambda}_j^c \left(\frac{1}{r_{ij}} - \frac{2\pi\delta(\mathbf{r}_{ij})\boldsymbol{\sigma}_i \cdot \boldsymbol{\sigma}_j}{3m_i m_j} \right), \quad (16)$$

m_i is the effective mass of the i -th quark. $\mathbf{r}_{ij} = \mathbf{r}_i - \mathbf{r}_j$ and $r_{ij} = |\mathbf{r}_i - \mathbf{r}_j|$. $\boldsymbol{\lambda}^c$ and $\boldsymbol{\sigma}$ represent the Gell-Mann matrices and the Pauli matrices, respectively. Dirac $\delta(\mathbf{r}_{ij})$ function comes out in the deduction of the interaction between point-like quarks, when not treated perturbatively, which leads to collapse [36]. Therefore, the $\delta(\mathbf{r}_{ij})$ function can be regularized in the form [37]

$$\delta(\mathbf{r}_{ij}) \rightarrow \frac{1}{4\pi r_{ij} r_0^2(\mu_{ij})} e^{-\frac{r_{ij}}{r_0(\mu_{ij})}}, \quad (17)$$

where $r_0(\mu_{ij}) = \frac{r_0}{\mu_{ij}}$, in which r_0 is an adjustable model parameter and μ_{ij} is the reduced mass of two interacting particles. This regularization is justified based on the finite size of the constituent quarks and should be therefore flavor dependent [38].

The quark-gluon coupling constant takes an effective scale-dependent form,

$$\alpha_s(\mu_{ij}^2) = \frac{\alpha_0}{\ln \frac{\mu_{ij}^2}{\Lambda_0^2}}, \quad (18)$$

Λ_0 and α_0 are adjustable model parameters.

To sum up, the completely Hamiltonian of the MCFTM for the mesons, baryons and hidden charm pentaquark states can be presented as

$$H_n = \sum_{i=1}^n \left(m_i + \frac{\mathbf{p}_i^2}{2m_i} \right) - T_c + \sum_{i<j}^n V_{ij}^{oge} + V_{min}^{con}(n). \quad (19)$$

T_c is the center-of-mass kinetic energy and should be deducted; \mathbf{p}_i is the momentum of the i -th quark.

III. WAVEFUNCTIONS

The total wavefunction $\Phi_{IJ}^{P_{cs}}$ of the pentaquark ground state $[nn][cs]\bar{c}$ ($n = u$ and d) with well-defined isospin I

and angular momentum J reads

$$\Phi_{IJ}^{P_{cs}} = \sum_{\delta} c_{\delta} \left[\left[\Psi_{csi}^{[nn]} \Psi_{csi}^{[cs]} \Psi_{csi}^{\bar{c}} \right]_{IS} F(\mathbf{r}, \mathbf{R}, \boldsymbol{\lambda}, \boldsymbol{\rho}) \right]_{IJ}, \quad (20)$$

where all []s represent all possible Clebsch-Gordan (C-G) coupling. Ψ_{csi} s are the color-spin-isospin (csi) wave functions and can be written as the product of the wave functions of color ψ_c , isospin ω_i and spin χ_s ,

$$\Psi_{csi}^{[nn]} = \psi_c^{[nn]} \chi_{ss_z}^{[nn]} \omega_{ii_z}^{[nn]}, \quad \Psi_{csi}^{[cs]} = \psi_c^{[cs]} \chi_{ss_z}^{[cs]} \omega_{ii_z}^{[cs]}, \quad (21)$$

$$\Psi_{csi}^{\bar{c}} = \psi_c^{\bar{c}} \chi_{ss_z}^{\bar{c}} \omega_{ii_z}^{\bar{c}}. \quad (22)$$

A set of Jacobi coordinates \mathbf{r} , \mathbf{R} , $\boldsymbol{\lambda}$, and $\boldsymbol{\rho}$ are used to describe the relative motions in the state P_{cs} ,

$$\mathbf{r} = \mathbf{r}_1 - \mathbf{r}_2, \quad \mathbf{R} = \mathbf{r}_3 - \mathbf{r}_4, \quad \boldsymbol{\lambda} = \frac{\mathbf{r}_1 + \mathbf{r}_2}{2} - \mathbf{r}_5, \quad (23)$$

$$\boldsymbol{\rho} = \frac{m_n \mathbf{r}_1 + m_n \mathbf{r}_2 + m_c \mathbf{r}_5}{2m_n + m_c} - \frac{m_c \mathbf{r}_3 + m_s \mathbf{r}_4}{m_s + m_c}. \quad (24)$$

Only the ground states are investigated in this work. The total spatial wave function $F(\mathbf{r}, \mathbf{R}, \boldsymbol{\lambda}, \boldsymbol{\rho})$ can be separated into a product of four relative motion wave functions

$$F(\mathbf{r}, \mathbf{R}, \boldsymbol{\lambda}, \boldsymbol{\rho}) = \phi_{00}(\mathbf{r})\phi_{00}(\mathbf{R})\phi_{00}(\boldsymbol{\lambda})\phi_{00}(\boldsymbol{\rho}). \quad (25)$$

According to the Gaussian expansion method (GEM) [39], the relative motion wave function $\phi_{lm}(\mathbf{x})$, where \mathbf{x} stands for \mathbf{r} , \mathbf{R} , $\boldsymbol{\lambda}$, and $\boldsymbol{\rho}$, can be expanded as the superposition of many different size (ν_n) Gaussian functions with well-defined orbital angular momentum,

$$\phi_{lm}(\mathbf{x}) = \sum_{n=1}^{n_{max}} c_n N_{nl} x^l e^{-\nu_n x^2} Y_{lm}(\hat{\mathbf{x}}) \quad (26)$$

Gaussian size parameters are taken as geometric progression,

$$\nu_n = \frac{1}{r_n^2}, \quad r_n = r_1 a^{n-1}, \quad a = \left(\frac{r_{n_{max}}}{r_1} \right)^{\frac{1}{n_{max}-1}} \quad (27)$$

N_{nl} is normalized coefficient and c_n is a variation coefficient determined by the model dynamics. With $r_1 = 0.2$ fm, $r_{n_{max}} = 2.0$ fm and $n_{max} = 7$, the converged numerical results can be achieved in the present work.

The spin wave functions $\chi_{ss_z}^{[nn]}$ of the diquark $[nn]$ can be written as

$$\chi_{10}^{[nn]} = \frac{1}{\sqrt{2}}(\uparrow\downarrow + \downarrow\uparrow), \quad \chi_{11}^{[nn]} = \uparrow\uparrow, \quad (28)$$

$$\chi_{1-1}^{[nn]} = \downarrow\downarrow, \quad \chi_{00}^{[nn]} = \frac{1}{\sqrt{2}}(\uparrow\downarrow - \downarrow\uparrow). \quad (29)$$

where \uparrow and \downarrow represent spin up and spin down, respectively. The wave functions $\chi_{ss_z}^{[cs]}$ of the diquark $[cs]$ are

exactly same with $\chi_{ssz}^{[nn]}$. The wave functions $\chi_{ssz}^{[\bar{c}]}$ of the antiquark \bar{c} read

$$\chi_{\frac{1}{2}\frac{1}{2}}^{\bar{c}} = \uparrow, \chi_{\frac{1}{2}-\frac{1}{2}}^{\bar{c}} = \downarrow. \quad (30)$$

The total spin wave function of the state P_{cs} with spin S and z -component S_z can be obtained by the following Clebsch-Gordan coupling

$$\chi_{SS_z}^{P_{cs}} = \chi_{ssz}^{[nn]} \oplus \chi_{ssz}^{[cs]} \oplus \chi_{ssz}^{\bar{c}}, \quad (31)$$

The isospin wave functions $\omega_{iiz}^{[nn]}$, $\omega_{iiz}^{[cs]}$ and $\omega_{iiz}^{\bar{c}}$ can be expressed as

$$\omega_{10}^{[nn]} = \frac{1}{\sqrt{2}}(ud + du), \omega_{11}^{[nn]} = uu, \omega_{1-1}^{[nn]} = dd, \quad (32)$$

$$\omega_{00}^{[nn]} = \frac{1}{\sqrt{2}}(ud - du), \omega_{00}^{[cs]} = cs, \omega_{00}^{\bar{c}} = \bar{c}. \quad (33)$$

The isospin of the state P_{cs} is determined by the diquark $[nn]$ because those of the diquarks $[cs]$ and \bar{c} are zero. The total isospin wave function therefore reads

$$\omega_{II_z}^{P_{cs}} = \omega_{II_z}^{[nn]} \omega_{00}^{[cs]} \omega_{00}^{\bar{c}}, \quad (34)$$

The color wave functions of the diquark $[nn]$ can be antisymmetrical color $\bar{\mathbf{3}}$ and symmetrical color $\mathbf{6}$ representation, their explicit component expressions read

$$\psi_{\bar{\mathbf{3}}_1}^{[nn]} = \frac{1}{\sqrt{2}}(rg - gr), \psi_{\bar{\mathbf{3}}_2}^{[nn]} = \frac{1}{\sqrt{2}}(gb - bg), \quad (35)$$

$$\psi_{\bar{\mathbf{3}}_3}^{[nn]} = \frac{1}{\sqrt{2}}(br - rb), \psi_{\mathbf{6}_1}^{[nn]} = rr, \quad (36)$$

$$\psi_{\mathbf{6}_2}^{[nn]} = \frac{1}{\sqrt{2}}(rg + gr), \psi_{\mathbf{6}_3}^{[nn]} = \frac{1}{\sqrt{2}}(rb + br), \quad (37)$$

$$\psi_{\mathbf{6}_4}^{[nn]} = gg, \psi_{\mathbf{6}_5}^{[nn]} = \frac{1}{\sqrt{2}}(gb + bg), \psi_{\mathbf{6}_6}^{[nn]} = bb \quad (38)$$

Those of the diquark $[cs]$ are exactly same with the diquark $[nn]$. The antiquark \bar{c} is in color $\bar{\mathbf{3}}$ and read

$$\psi_{\bar{\mathbf{3}}_1}^{\bar{c}} = \bar{r}, \psi_{\bar{\mathbf{3}}_2}^{\bar{c}} = \bar{g}, \psi_{\bar{\mathbf{3}}_3}^{\bar{c}} = \bar{b}. \quad (39)$$

The diquarks $\psi_{\bar{c}}^{[nn]}$ and $\psi_{\bar{c}}^{[cs]}$ must couple into a tetraquark state in color $\mathbf{3}$ according to the requirement of overall color singlet of the state P_{cs} . Therefore, the total color singlet wave function can be expressed as

$$\psi_c^{P_{cs}} = \frac{1}{\sqrt{3}} \left(\psi_{\bar{\mathbf{3}}_1}^{[nn][cs]} \psi_{\bar{\mathbf{3}}_1}^{\bar{c}} + \psi_{\bar{\mathbf{3}}_2}^{[nn][cs]} \psi_{\bar{\mathbf{3}}_2}^{\bar{c}} + \psi_{\bar{\mathbf{3}}_3}^{[nn][cs]} \psi_{\bar{\mathbf{3}}_3}^{\bar{c}} \right). \quad (40)$$

There are the following three different coupling ways of the diquark $[nn]$ and $[cs]$ into a tetraquark state $\psi_{\mathbf{3}}^{[nn][cs]}$, case A: $\psi_{\bar{\mathbf{3}}}^{[nn]} \otimes \psi_{\bar{\mathbf{3}}}^{[cs]}$; case B: $\psi_{\mathbf{6}}^{[nn]} \otimes \psi_{\mathbf{3}}^{[cs]}$ and case C:

$\psi_{\bar{\mathbf{3}}}^{[nn]} \otimes \psi_{\mathbf{6}}^{[cs]}$. For the case A, its explicit component expressions read

$$\psi_{\bar{\mathbf{3}}_1}^{[nn][cs]} = \frac{1}{\sqrt{2}} \psi_{\bar{\mathbf{3}}_1}^{[nn]} \psi_{\bar{\mathbf{3}}_3}^{[cs]} - \frac{1}{\sqrt{2}} \psi_{\bar{\mathbf{3}}_3}^{[nn]} \psi_{\bar{\mathbf{3}}_1}^{[cs]}, \quad (41)$$

$$\psi_{\bar{\mathbf{3}}_2}^{[nn][cs]} = \frac{1}{\sqrt{2}} \psi_{\bar{\mathbf{3}}_1}^{[nn]} \psi_{\bar{\mathbf{3}}_2}^{[cs]} - \frac{1}{\sqrt{2}} \psi_{\bar{\mathbf{3}}_2}^{[nn]} \psi_{\bar{\mathbf{3}}_1}^{[cs]}, \quad (42)$$

$$\psi_{\bar{\mathbf{3}}_3}^{[nn][cs]} = \frac{1}{\sqrt{2}} \psi_{\bar{\mathbf{3}}_3}^{[nn]} \psi_{\bar{\mathbf{3}}_2}^{[cs]} - \frac{1}{\sqrt{2}} \psi_{\bar{\mathbf{3}}_2}^{[nn]} \psi_{\bar{\mathbf{3}}_3}^{[cs]}. \quad (43)$$

For the case B, its explicit component expressions read

$$\psi_{\bar{\mathbf{3}}_1}^{[nn][cs]} = \frac{\sqrt{2}}{2} \psi_{\bar{\mathbf{6}}_1}^{[nn]} \psi_{\bar{\mathbf{3}}_2}^{[cs]} - \frac{1}{2} \psi_{\bar{\mathbf{6}}_2}^{[nn]} \psi_{\bar{\mathbf{3}}_3}^{[cs]} + \frac{1}{2} \psi_{\bar{\mathbf{6}}_3}^{[nn]} \psi_{\bar{\mathbf{3}}_1}^{[cs]}, \quad (44)$$

$$\psi_{\bar{\mathbf{3}}_2}^{[nn][cs]} = \frac{1}{2} \psi_{\bar{\mathbf{6}}_2}^{[nn]} \psi_{\bar{\mathbf{3}}_2}^{[cs]} - \frac{\sqrt{2}}{2} \psi_{\bar{\mathbf{6}}_4}^{[nn]} \psi_{\bar{\mathbf{3}}_3}^{[cs]} + \frac{1}{2} \psi_{\bar{\mathbf{6}}_5}^{[nn]} \psi_{\bar{\mathbf{3}}_1}^{[cs]}, \quad (45)$$

$$\psi_{\bar{\mathbf{3}}_3}^{[nn][cs]} = \frac{1}{2} \psi_{\bar{\mathbf{6}}_3}^{[nn]} \psi_{\bar{\mathbf{3}}_2}^{[cs]} - \frac{1}{2} \psi_{\bar{\mathbf{6}}_5}^{[nn]} \psi_{\bar{\mathbf{3}}_3}^{[cs]} + \frac{\sqrt{2}}{2} \psi_{\bar{\mathbf{6}}_6}^{[nn]} \psi_{\bar{\mathbf{3}}_1}^{[cs]}. \quad (46)$$

For the case C, its explicit component expressions read

$$\psi_{\bar{\mathbf{3}}_1}^{[nn][cs]} = \frac{\sqrt{2}}{2} \psi_{\bar{\mathbf{3}}_2}^{[nn]} \psi_{\bar{\mathbf{6}}_1}^{[cs]} - \frac{1}{2} \psi_{\bar{\mathbf{3}}_3}^{[nn]} \psi_{\bar{\mathbf{6}}_2}^{[cs]} + \frac{1}{2} \psi_{\bar{\mathbf{3}}_1}^{[nn]} \psi_{\bar{\mathbf{6}}_3}^{[cs]}, \quad (47)$$

$$\psi_{\bar{\mathbf{3}}_2}^{[nn][cs]} = \frac{1}{2} \psi_{\bar{\mathbf{3}}_2}^{[nn]} \psi_{\bar{\mathbf{6}}_2}^{[cs]} - \frac{\sqrt{2}}{2} \psi_{\bar{\mathbf{3}}_3}^{[nn]} \psi_{\bar{\mathbf{6}}_4}^{[cs]} + \frac{1}{2} \psi_{\bar{\mathbf{3}}_1}^{[nn]} \psi_{\bar{\mathbf{6}}_5}^{[cs]}, \quad (48)$$

$$\psi_{\bar{\mathbf{3}}_3}^{[nn][cs]} = \frac{1}{2} \psi_{\bar{\mathbf{3}}_2}^{[nn]} \psi_{\bar{\mathbf{6}}_3}^{[cs]} - \frac{1}{2} \psi_{\bar{\mathbf{3}}_3}^{[nn]} \psi_{\bar{\mathbf{6}}_5}^{[cs]} + \frac{\sqrt{2}}{2} \psi_{\bar{\mathbf{3}}_1}^{[nn]} \psi_{\bar{\mathbf{6}}_6}^{[cs]}. \quad (49)$$

The diquark is a spatially extended object with various color-spin-isospin-orbit combinations [40]. For the sake of convenience, we define the color quantum number $c = 0$ and $c = 1$ for the diquark in the color $\bar{\mathbf{3}}$ and $\mathbf{6}$ representation, respectively. For the identical diquarks $[dd]$, $[ud]$ and $[ud]$, their spin s , isospin i , orbit angular excitation l , and color c obey the constraint $s + i + l + c = \text{even}$ to satisfy the Pauli principle. The spin singlet, isospin singlet and color triplet diquark with $l = 0$ is often called the good diquark. Other combinations are sometimes called bad diquarks. For the strange diquark $[ss]$, its spin s , isospin i , orbit angular excitation l , and color c obey the constraint $s + i + l + c = \text{odd}$ because its isospin is symmetrical. In this work, we are only interested in the ground states, namely $l = 0$. The diquarks $[cu]$, $[cd]$ and $[cs]$ are not identical particles so that their quantum numbers are not constrained.

The diquark $[nn]$ has four possible antisymmetrical spin-isospin-color combinations,

$$\Psi_{csi}^{[nn]} = \Psi_{\mathbf{3}00}^{[nn]}, \Psi_{\bar{\mathbf{3}}11}^{[nn]}, \Psi_{\mathbf{6}01}^{[nn]}, \Psi_{\bar{\mathbf{6}}10}^{[nn]}. \quad (50)$$

According to the total spin and isospin of the state P_{cs} and color configurations, one can obtain all possible wave

functions, which are represented by the δ in Eq. (20). Its corresponding coefficient c_δ can be determined by the model dynamics. For example, the total wave function of the state P_{cs} with $0\frac{1}{2}^-$ has seven possibilities.

The total wave function $\Phi_{IJ}^{P_{css}}$, $P_{css} = [ss][cn]\bar{c}$, is exactly same with that of the state P_{cs} with isospin $I = 1$ because the flavor parts of the diquarks $[ss]$ and $[nm]$ are both symmetrical. For the same reason, the total wave function $\Phi_{IJ}^{P_{csss}}$, $P_{csss} = [ss][cs]\bar{c}$, is exactly same with that of the state $[nm][cn]\bar{c}$ with isospin $I = \frac{3}{2}$, which can be obtained in the previous work [18].

Using the same procedure with the diquark configuration, one can easily construct the wave functions of the state $[qqq][c\bar{c}]$ with color octet configuration, which can also be achieved in ref. [41] so that those are omitted here. Note that it is difficult to construct the wave functions of the pentagon structure in the quark level. In this work, we first employ the wave functions of the diquark structure to calculate the mass of the pentagon structure approximately. More reliable estimation is left for further research in future.

IV. NUMERICAL RESULTS AND DISCUSSIONS

A. Parameters and conventional hadron spectra

We take the ϕ and ω mesons as the ideal mixing of the SU(3) singlet ω_0 and the octet ω_8 states in this work, namely $\omega = \frac{1}{\sqrt{2}}(u\bar{u} + d\bar{d})$, $\phi = s\bar{s}$ and the ideal mixing angle $\theta_V = 35.3^\circ$. We can obtain the masses of meson and baryon ground states by approximately strict solving two-body and three-body Schrödinger equations in the MCFTM. We use the mean square error

$$\Delta = \sum_{i=1}^N \frac{w_i(M_i - m_i)^2}{N} \quad (51)$$

to fit the mass spectra and to determine the adjustable parameters and their errors in the Minuit program [18]. N is the total number of mesons and baryons. M_i is the experimental mass of the i th meson or baryon and m_i is its predicted mass in the model. w_i is its corresponding weight for fitting mass spectrum better. For the heavy parts, their weights are equal to 1. For the light parts, especially for π and K mesons, their values are greater than 1, such as 2 and 3.

Finally, we can obtain the optima parameters and spectra, which are presented in Tables II and III, respectively. Moreover, we can also arrive at the mass errors for mesons, baryons and pentaquark states, just several MeV [18], introduced by the errors of the parameters. From Table III, one can see that the meson and baryon ground states, from the lightest π to the heaviest $\Upsilon(1S)$, can be simultaneously accommodated in the model very well with only a few adjustable model parameters. The

fact indicates that the multibody confinement potential based on the color flux-tube picture may be a valid dynamical mechanism in the phenomenological description of the properties of meson and baryon states. Of course, other properties of those states need further study, which is left for the future work.

TABLE II: Adjustable model parameters, quark mass and Λ_0 unit in MeV, k unit in $\text{MeV}\cdot\text{fm}^{-2}$, r_0 unit in $\text{MeV}\cdot\text{fm}$ and α_0 is dimensionless.

Para.	$m_{u,d}$	m_s	m_c	m_b	k	α_0	Λ_0	r_0
Valu.	230	473	1701	5047	700	4.69	30.24	81.48

TABLE III: Conventional meson and baryon spectra, unit in MeV.

State	π	ρ	ω	K	K^*	ϕ	D^\pm
Theo.	137	762	762	494	922	1058	1879
PDG	139	770	780	496	896	1020	1869
State	D^*	D_s^\pm	D_s^*	η_c	J/Ψ	B^0	B^*
Theo.	2039	1952	2144	2949	3128	5285	5343
PDG	2007	1968	2112	2980	3097	5280	5325
State	B_s^0	B_s^*	B_c	B_c^*	η_b	$\Upsilon(1S)$	
Theo.	5352	5429	6254	6396	9374	9536	
PDG	5366	5416	6277	...	9391	9460	
State	N	Δ	Σ	Σ^*	Ξ	Ξ^*	Λ
Theo.	945	1239	1204	1391	1345	1537	1128
PDG	939	1232	1195	1385	1315	1530	1115
State	Ω	Σ_c	Σ_c^*	Ξ_c	Ξ_c^*	Ω_c^0	Ω_c^{*0}
Theo.	1677	2437	2508	2460	2626	2703	2774
PDG	1672	2445	2520	2466	2645	2695	2766
State	Λ_c^+	Σ_b	Σ_b^*	Ξ_b	Ξ_b^*	Ω_b^-	Λ_b^0
Theo.	2278	5786	5812	5765	5817	6034	5596
PDG	2285	5808	5830	5790	...	6071	5620

B. $qqqc\bar{c}$ spectrum

So far, the baryon-meson molecular descriptions of the P_c and P_{cs} states seem to prevail over other possibilities in various theoretical framework because of the proximity of their masses to the baryon-meson thresholds [29]. However, it does not mean that other possibilities can be excluded completely. According to QCD, the hidden color components are allowed in addition to the color singlet component in the pentaquark states. In a large extent, the pentaquark states should be a mixture of all possible color configurations. In this work, we first attempt to explore the natures of the pentaquark states from the perspective of hidden color components. Another reason is the absence of the one-boson-exchange interaction in the MCFTM, which is widely accepted as the binding mechanism of molecular states from the phenomenological model point of view. The mixing between the color singlet and hidden color components deserves

further investigation in future.

Next, we move on to the investigation on the properties of the hidden color pentaquark states $qqqc\bar{c}$ in the MCFTM. The P -parity of the states is negative because we are interested in the ground states. In this way, the spin-parity assignment of the pentaquark states should be $\frac{1}{2}^-$, $\frac{3}{2}^-$ and $\frac{5}{2}^-$. The total isospin of the pentaquark states depends on their specific quark content. We can achieve the mass of the states with all possible isospin and spin-parity and three various color structures, diquark, octet and pentagon, by solving the five-body Schrödinger equation with the well-defined trial wave functions. We present their mass spectrum in Table IV, in which E_d , E_o , and E_p respectively represent the masses of the diquark, octet and pentagon structures.

TABLE IV: The mass of the ground state $qqqc\bar{c}$ with IJ^P and various color structures, unit in MeV.

J^P	$nnnc\bar{c}, I = \frac{1}{2}$			$nnnc\bar{c}, I = \frac{3}{2}$			$nnsc\bar{c}, I = 0$		
	E_o	E_d	E_p	E_o	E_d	E_p	E_o	E_d	E_p
$\frac{1}{2}^-$	4402	4344	4303	4620	4581	4532	4512	4487	4463
$\frac{3}{2}^-$	4473	4405	4369	4661	4622	4573	4611	4585	4570
$\frac{5}{2}^-$	4616	4569	4516	4743	4707	4666	4911	4884	4846
J^P	$nnsc\bar{c}, I = 1$			$nssc\bar{c}, I = \frac{1}{2}$			$sssc\bar{c}, I = 0$		
	E_o	E_d	E_p	E_o	E_d	E_p	E_o	E_d	E_p
$\frac{1}{2}^-$	4617	4595	4579	4784	4750	4730	5047	5019	4985
$\frac{3}{2}^-$	4715	4690	4675	4877	4839	4823	5074	5048	5017
$\frac{5}{2}^-$	4850	4822	4810	5008	4963	4954	5140	5115	5089

TABLE V: The average values $\langle V^{oge} \rangle$, $\langle V^{con} \rangle$, and $\langle T \rangle$ in the three structures, T stands for kinetic energy, unit in MeV.

Flavor	$nnnc\bar{c}$			$nnsc\bar{c}$		
IJ^P	$\frac{1}{2} \frac{1}{2}^-$			$0 \frac{1}{2}^-$		
Stru.	octet	diquark	pentagon	octet	diquark	pentagon
$\langle V^{oge} \rangle$	-2111	-2099	-2074	-1999	-1973	-1965
$\langle V^{con} \rangle$	1756	1710	1673	1628	1594	1574
$\langle T \rangle$	664	640	614	547	529	518

It can be seen from Table IV that the color structures can induce the mass splitting like the color-magnetic interaction does. The masses E_o , E_d and E_p are close and their order is $E_o > E_d > E_p$. The mass difference between the two adjacent items is several tens MeV, which mainly come from the different type of confinement potential determined by the color structure, see Table V. The confinement potential of the octet structure is bigger than that of the diquark structure because there is one piece of stronger color **8**-dimension color flux-tube than **3**-dimension one. That of the ring-like pentagon structure is lowest because the structure is easier to shrink into a compact multi-quark state relative to the octet and diquark structures.

C. P_c and P_{cs} states observed by the LHCb Collaboration

Matching the masses predicted by the MCFTM with the experimental data of the states, we present the possible interpretation on the IJ^P and color structures of the states in Table VI. At first glance, all of the states can be accommodated in the model. In addition, we also calculate the average distances, smaller than 1 fm, between any two quarks using the eigen wave function of the states. In this way, the states should be compact in the model because of the five-body confinement potential.

One can find from Table VI that the mass of the state $uudc\bar{c}$ with $\frac{1}{2} \frac{1}{2}^-$ and pentagon structure is 4303 MeV, which is very close to the experimental data of the state $P_c(4312)^+$. In this way, its main component can be described as the compact state $uudc\bar{c}$ with $\frac{1}{2} \frac{1}{2}^-$ and pentagon structure in the model. No matter what its structure is, the state seems to prefer the spin-parity assignment of $\frac{1}{2}^-$ in many theoretical frameworks [42–44, 46, 47]. Conversely, the other spin-parity assignments of $\frac{1}{2}^+$ [25, 26] and $\frac{3}{2}^-$ [48] were also proposed.

The mass of the state $uudc\bar{c}$ with $\frac{1}{2} \frac{1}{2}^-$ and diquark structure is 4344 MeV, which is highly consistent with the experimental data of the state $P_c(4337)^+$. The states $P_c(4312)^+$ and $P_c(4337)^+$ have the same assignment of spin-parity in the model. However, the state $P_c(4312)^+$ is pentagon structure while the state $P_c(4337)^+$ is diquark structure. Therefore, they should be so-called QCD isomers in the model. For the two states, Yan et al proposed three possible explanations [49]: the state $P_c(4337)^+$ is a χ_{c0p} bound state with $\frac{1}{2}^+$; the state $P_c(4337)^+$ is a $\bar{D}\Sigma_c$ molecule with $\frac{1}{2}^-$ while the state $P_c(4312)^+$ is a $\bar{D}^*\Lambda_c$ molecule with $\frac{1}{2}^-$ or $\frac{3}{2}^-$; the states $P_c(4312)^+$ and $P_c(4337)^+$ are the coupled channel systems $\bar{D}^*\Lambda_c - \bar{D}\Sigma_c$ with $\frac{1}{2}^-$ and $\bar{D}^*\Lambda_c - \bar{D}\Sigma_c^*$ with $\frac{3}{2}^-$, respectively. Nakamura et al described the states $P_c(4312)^+$ and $P_c(4337)^+$ as interfering $\bar{D}\Sigma_c$ and $\bar{D}^*\Lambda_c$ cusps with $\frac{1}{2}^-$ [50].

The states $uudc\bar{c}$ with $\frac{1}{2} \frac{3}{2}^-$ and pentagon and diquark structure have masses of 4369 MeV and 4405 MeV in the MCFTM, respectively, both of which are in agreement with the experimental data of the state $P_c(4380)^+$. The model therefore approves the description of the state as the compact state $uudc\bar{c}$ with $\frac{1}{2} \frac{3}{2}^-$ and pentagon or diquark structure. The molecule structure [51], the diquark structure [52], and the diquark-triquark structure [53] in various theoretical frameworks also supported the spin-parity assignment of $\frac{3}{2}^-$. In addition, the state $uudc\bar{c}$ with $\frac{1}{2} \frac{1}{2}^-$ and octet structure is around 4402 MeV, which is not far away from that of the state $P_c(4380)^+$. We can not rule out the possibility that the main component of the state $P_c(4380)^+$ may be the state $uudc\bar{c}$ with $\frac{1}{2} \frac{1}{2}^-$ and octet structure.

The states $uudc\bar{c}$ with $\frac{1}{2} \frac{3}{2}^-$ and diquark and octet

TABLE VI: Possible isospin-spin-parity and structure assignments of the P_c and P_{cs} states and their average distance $\langle \mathbf{r}_{ij}^2 \rangle^{\frac{1}{2}}$ in the MCFTM, unit in fm.

Flavor	IJ^P	Structure	Mass	Candidate	$\langle \mathbf{r}_{12}^2 \rangle^{\frac{1}{2}}$	$\langle \mathbf{r}_{13}^2 \rangle^{\frac{1}{2}}$	$\langle \mathbf{r}_{23}^2 \rangle^{\frac{1}{2}}$	$\langle \mathbf{r}_{14}^2 \rangle^{\frac{1}{2}}$	$\langle \mathbf{r}_{24}^2 \rangle^{\frac{1}{2}}$	$\langle \mathbf{r}_{34}^2 \rangle^{\frac{1}{2}}$	$\langle \mathbf{r}_{15}^2 \rangle^{\frac{1}{2}}$	$\langle \mathbf{r}_{25}^2 \rangle^{\frac{1}{2}}$	$\langle \mathbf{r}_{35}^2 \rangle^{\frac{1}{2}}$	$\langle \mathbf{r}_{45}^2 \rangle^{\frac{1}{2}}$
$uudc\bar{c}$	$\frac{1}{2} \frac{1}{2}^-$	pentagon	4303	$P_c(4312)^+$	0.90	0.90	0.90	0.75	0.75	0.75	0.76	0.76	0.76	0.37
$uudc\bar{c}$	$\frac{1}{2} \frac{1}{2}^-$	diquark	4344	$P_c(4337)^+$	0.90	0.90	0.90	0.75	0.75	0.75	0.76	0.76	0.76	0.37
$uudc\bar{c}$	$\frac{1}{2} \frac{3}{2}^-$	pentagon	4369	$P_c(4380)^+$	0.91	0.91	0.91	0.78	0.78	0.78	0.78	0.78	0.78	0.40
$uudc\bar{c}$	$\frac{1}{2} \frac{3}{2}^-$	diquark	4405	$P_c(4440)^+$	0.89	0.89	0.89	0.77	0.77	0.77	0.77	0.77	0.77	0.40
$uudc\bar{c}$	$\frac{1}{2} \frac{3}{2}^-$	octet	4475	$P_c(4457)^+$	0.89	0.89	0.89	0.77	0.77	0.77	0.77	0.77	0.77	0.40
$udsc\bar{c}$	$0 \frac{1}{2}^-$	pentagon	4463	$P_{cs}(4459)^0$	0.84	0.88	0.88	0.73	0.73	0.64	0.73	0.73	0.62	0.40

structures have masses of 4405 MeV and 4473 MeV, respectively, which are not far from the experimental data of the states $P_c(4440)^+$ and $P_c(4457)^+$. The deviations from their experimental central data are about 35 MeV and 18 MeV, respectively. In this way, the main components of the states $P_c(4440)^+$ and $P_c(4457)^+$ can be described as the compact states $uudc\bar{c}$ with diquark and octet structures in the model, respectively. However, they share the same isospin-spin-parity $\frac{1}{2} \frac{3}{2}^-$. Until now, even if ignoring their structures, their spin-parity have been highly controversial in the various theoretical frameworks, such as $\frac{3}{2}^-$ and $\frac{1}{2}^-$ [44], $\frac{1}{2}^-$ and $\frac{3}{2}^-$ [47], $\frac{3}{2}^+$ and $\frac{5}{2}^+$ [48], $\frac{3}{2}^-$ and $\frac{1}{2}^+$ [54], etc. Liu et al suggested that the discovery of the strange pentaquark molecular state $\bar{D}^{(*)}\Xi_c$ may be propitious to determine the spin of the states $P_c(4440)$ and $P_c(4457)$ in the molecular picture [55].

The strange state $nssc\bar{c}$ with $0 \frac{1}{2}^-$ and pentagon structure has a mass of 4463 MeV in the MCFTM, which is completely consistent with the experimental value of the state $P_{cs}(4459)^0$. Hence, the model supports the interpretation of the state as the compact state $nssc\bar{c}$ with $0 \frac{1}{2}^-$ and pentagon structure. Chiral quark model can describe the state as $\Xi'_c \bar{D}$ molecule with $0 \frac{1}{2}^-$ [56]. Regardless of the $\bar{D}^* \Xi_c$ molecular and diquark pictures, QCD sum rule supports that the spin-parity assignment of the state is $\frac{1}{2}^-$ [57–59]. Conversely, both of one-boson-exchange model and quasipotential Bethe-Salpeter equation favored the interpretation of the state as the molecular picture with $\frac{3}{2}^-$ [60, 61]. Furthermore, Du et al favored the actual existence of two resonances with spin $\frac{1}{2}$ and $\frac{3}{2}$ in the energy region of the state $P_{cs}(4459)^0$ in relation with the heavy-quark-spin symmetry [62]. In the hadro-charmonium model, the state $P_{cs}(4459)^0$ prefers the spin-parity assignment of $\frac{1}{2}^-$ or $\frac{3}{2}^-$ [26].

D. Other P_c , P_{cs} , P_{css} and P_{csss} states predicted by the MCFTM

We can describe the hidden charmed states $P_c(4312)^+$, $P_c(4337)^+$, $P_c(4380)^+$, $P_c(4440)^+$ and $P_c(4457)^+$ as the

lower spin and lower isospin members in the P_c family with various color configurations. We predict other possible states $qqqc\bar{c}$ with high spin $S = \frac{5}{2}$ and high isospin $I = \frac{3}{2}$ in the model. One can find from Table IV that the masses of the states with $\frac{1}{2} \frac{5}{2}^-$ are in the range of 4516 MeV to 4616 MeV. The masses of the states with $I = \frac{3}{2}$ spans from 4532 MeV to 4743 MeV, which changes with their spin and color flux-tube structures. Most of the states with $I = \frac{3}{2}$ are far away from their highest threshold $\Sigma_c^* D^*$.

Like the P_c family, the lowest state $P_{cs}(4459)^0$ indicates that there probably exist other members in the P_{cs} family. In the model, the other two P_{cs} states with $0 \frac{1}{2}^-$ and diquark and octet structures have masses of around 4500 MeV, see Table IV. The masses of the states with $0 \frac{3}{2}^-$ and three different structures range from 4570 MeV to 4610 MeV. The states with $1 \frac{1}{2}^-$ and $1 \frac{3}{2}^-$ are higher about 100 MeV than the states with $0 \frac{1}{2}^-$ and $0 \frac{3}{2}^-$, respectively. Conversely, the states with $1 \frac{5}{2}^-$ are lower several tens MeV than the states with $0 \frac{5}{2}^-$ because the diquark $[nn]$ with $I = 1$ is in color $\bar{\mathbf{3}}$ while the diquark $[nn]$ with $I = 0$ is in color $\mathbf{6}$. In general, the interaction in color $\bar{\mathbf{3}}$ is attractive while that in color $\mathbf{6}$ is repulsive. The states $nssc\bar{c}$ with $\frac{5}{2}^-$ are far away from the highest threshold $\Xi'_c D^*$.

The wave functions of the states P_{css} and those of the states P_{cs} with $I = 1$ have the same symmetry. Their mass difference, about 150 MeV, mainly come from the mass of s -quark. For the states P_{css} with $\frac{1}{2}^-$, their masses are in the range of 4730 MeV to 4784 MeV, which are close to the result, 4600 ± 175 MeV, predicted by the QCD sum rule method [64]. Wang et al predicted double strangeness molecular states $\Xi'_c \bar{D}_s^*$ with $\frac{5}{2}^-$ and $\Xi'_c \bar{D}_s^*$ with $\frac{3}{2}^-$ [65], which are much lower about 200 MeV than our results. The states $nssc\bar{c}$ with $\frac{5}{2}^-$ are far away from the highest threshold $\Omega_c^* D^*$ in the MCFTM.

The masses of the P_{csss} states are higher 400 MeV than those of the states P_c with $I = \frac{3}{2}$ also because of the mass of s -quark in the MCFTM. They are in the range of 4985 MeV to 5140 MeV and do not dramatically change with spin and color structures. All of the states $sssc\bar{c}$ are far

away from the threshold $\Omega_c^* D_s^*$.

V. SUMMARY

The observation of the hidden charmed pentaquark states P_c and P_{cs} by the LHCb Collaboration presents an extremely interesting spectrum. Their masses locate around the baryon-meson thresholds. However, there has not been a general consensus regarding their natures and structures until now. The baryon-meson molecular interpretation is the most popular one.

In this work, we make a systematical dynamical investigation on the hidden charm pentaquark states with the help of the high precision numerical method GEM in the multi-quark color flux-tube model. The model involves the multi-body confinement potential based on the color flux-tube picture in the lattice QCD. Different color structures, pentagon, diquark and octet structure, induce the QCD isomers, which have the close masses in the model. Like the color-magnetic interaction, such color structure effect can also induce mass splitting in the spectrum and make hadron world more fantastic.

The model shows a novel picture for the P_c and P_{cs} states. It can describe the states as the compact pentaquark states with different structures. The spin-parity of the group of $P_c(4312)^+$ and $P_c(4337)^+$ is $\frac{1}{2}^-$ while that of the group of $P_c(4380)^+$, $P_c(4440)^+$ and $P_c(4457)^+$ is $\frac{3}{2}^-$. Their structures are pentagon, diquark, pentagon,

diquark, and octet, respectively. The members in each group can be analogically called QCD isomers because of their the same spin-parity and quark content but different color structures. The singlet $P_{cs}(4459)^0$ has pentagon structure and spin-parity of $\frac{1}{2}^-$. The structure coupling effect in the QCD isomers should occur, which will be taken into account in the future. Note that our model conclusion just serves as one of possible theoretical suggestions. Proper identification of the structure and property of the states require more experimental and theoretical scrutiny. In addition, we also predict the P_{cs} , P_{css} and P_{csss} families in the model. We hope that these states can be searched in experiments in the future.

The five-body confinement potential, a collective degree of freedom, binds quarks to form the compact pentaquark states. It may shed light on our understanding of how quarks and gluons establish hadrons in the low-energy strong interactions.

Acknowledgments

Author thanks Prof. S.L. Zhu for helpful discussions. This research is partly supported by the Chongqing Natural Science Foundation under Project No. cstc2019jcyj-msxmX0409 and Fundamental Research Funds for the Central Universities under Contracts No. SWU118111.

-
- [1] M. Gell-Mann, Phys. Lett. **8**, 214 (1964).
 - [2] M. Amarian, Arxiv: 2201.04885 [hep-ex].
 - [3] J.J. Wu, R. Molina, E. Oset, and B.S. Zou, Phys. Rev. Lett. **105**, 232001 (2010).
 - [4] W.L. Wang, F. Huang, Z.Y. Zhang, and B.S. Zou, Phys. Rev. C **84**, 015203 (2011).
 - [5] J.J. Wu, T.S. H. Lee, and B.S. Zou, Phys. Rev. C **85**, 044002 (2012).
 - [6] C.W. Xiao, J. Nieves, and E. Oset, Phys. Rev. D **88**, 056012 (2013).
 - [7] M. Karliner and J.L. Rosner, Phys. Rev. Lett. **115**, 122001 (2015).
 - [8] R. Aaij et al. (LHCb Collaboration), Phys. Rev. Lett. **115**, 072001 (2015).
 - [9] R. Aaij et al. (LHCb Collaboration), Phys. Rev. Lett. **122**, 222001 (2019).
 - [10] R. Aaij et al. (LHCb Collaboration), Sci.Bull. **66**, 1278 (2021).
 - [11] R. Aaij et al. (LHCb Collaboration), Phys. Rev. Lett. **128**, 062001 (2022).
 - [12] M.L. Du, V. Baru, F.K. Guo, C. Hanhart, Ulf-G. Meißner, J.A. Oller, and Q. Wang, Phys. Rev. Lett. **124**, 072001 (2020).
 - [13] B. Wang, L. Meng, and S.L. Zhu, JHEP **11**, 108 (2019).
 - [14] M.Z. Liu, Y.W. Pan, F.Z. Peng, M.S. Sanchez, L.S. Geng, A. Hosaka, and M.P. Valderrama, Phys. Rev. Lett. **122**, 242001 (2019).
 - [15] H.X. Chen, W. Chen, X. Liu, T.G. Steele, and S.L. Zhu, Phys. Rev. Lett. **115**, 172001 (2015).
 - [16] R. Chen, X. Liu, X.Q. Li, and S.L. Zhu, Phys. Rev. Lett. **115**, 132002 (2015).
 - [17] E. Santopinto and A. Giachino, Phys. Rev. D **96**, 014014 (2017).
 - [18] C.R. Deng, J.L. Ping, H.X. Huang, and F. Wang, Phys. Rev. D **95**, 014031 (2017).
 - [19] R.L. Zhu and C.F. Qiao, Phys. Lett. B **756**, 259 (2016).
 - [20] R.F. Lebed, Phys. Lett. B **749**, 454 (2015).
 - [21] A. Ali, I. Ahmed, M.J. Aslam, A.Y. Parkhomenko, and A. Rehman, JHEP **10**, 256 (2019).
 - [22] F. Stancu, Phys. Rev. D **104**, 054050 (2021).
 - [23] F.K. Guo, U.G. Meissner, W. Wang, Z. Yang, Phys. Rev. D **92**, 071502 (2015).
 - [24] X.H. Liu, Q. Wang, Q. Zhao, Phys. Lett. B **757**, 231 (2016).
 - [25] M.I. Eides, V.Y. Petrov, and M.V. Polyakov, Mod. Phys. Lett. A **35**, 2050151 (2020).
 - [26] J. Ferretti and E. Santopinto, arXiv: 2111.08650 [hep-ph].
 - [27] C. Fernández-Ramírez, A. Pilloni, M. Albaladejo, A. Jackura, V. Mathieu, M. Mikhasenko, J.A. Silva-Castro, and A.P. Szczepaniak, Phys. Rev. Lett. **123**, 092001 (2019).
 - [28] S.X. Nakamura, PoS CHARM2020, **029** (2021).
 - [29] Y.R. Liu, H.X. Chen, W. Chen, X. Liu, and S.L. Zhu, Prog.

- Part. Nucl. Phys. **107**, 237 (2019); N. Brambilla, S. Eidelman, C. Hanhart, A. Nefediev, C.P. Shen, C.E. Thomas, A. Vairo, and C.Z. Yuan, Phys. Rep. **873**, 1(2020); F.K. Guo, X.H. Liu, and S. Sakai, Prog. Part. Nucl. Phys. **112**, 103757 (2020); H.X. Chen, W. Chen, X. Liu, Y.R. Liu, and S.L. Zhu, arXiv: 2204.02649 [hep-ph]; L. Meng, B. Wang, G.J. Wang, and S.L. Zhu, arXiv: 2204.08716 [hep-ph].
- [30] Y.W. Pan, M.Z. Liu, F.Z. Peng, M.S. Sánchez, L.S. Geng, and M.P. Valderrama, Phys. Rev. D **102**, 011504 (2020)
- [31] T.T. Takahashi, H. Suganuma, Y. Nemoto, and H. Matsufuru, Phys. Rev. D **65**, 114509 (2002).
- [32] F. Okiharu, H. Suganuma, T.T. Takahashi, Phys. Rev. Lett. **94**, 192001 (2005); J.L. Ping, C.R. Deng, F. Wang, and T. Goldman, Phys. Lett. B **659**, 607 (2008).
- [33] J.M. Richard, arXiv: 1205.4326 [hep-ph].
- [34] C.R. Deng, H. Chen, and J.L. Ping, Phys. Rev. D **103**, 014001 (2021); C.R. Deng, H. Chen, and J.L. Ping, Eur. Phys. J. A **56**, 9 (2020).
- [35] G.S. Bali, Phys. Rev. D **62**, 114503 (2000); C. Semay, Eur. Phys. J. A **22**, 353 (2004); N. Cardoso, M. Cardoso, and P. Bicudo, Phys. Lett. B **710**, 343 (2012).
- [36] R.K. Bhaduri, L.E. Cohler, and Y. Nogami, Phys. Rev. Lett. **44**, 1369 (1980).
- [37] J. Vijande, F. Fernandez, and A. Valcarce, J. Phys. G **31**, 481 (2005).
- [38] J. Weinstein and N. Isgur, Phys. Rev. D **27**, 588 (1983).
- [39] E. Hiyama, Y. Kino, and M. Kamimura, Prog. Part. Nucl. Phys. **51** 223 (2003).
- [40] C.R. Deng and S.L. Zhu, arXiv: 2204.11079 [hep-ph].
- [41] G. Yang, J. Ping, and J. Segovia, Phys. Rev. D **99**, 014035 (2019).
- [42] H.X. Chen, W. Chen and S.L. Zhu, Phys. Rev. D **100**, 051501 (2019); J.R. Zhang, Eur. Phys. J. C **79**, 1001 (2019); K. Azizi, Y. Sarac, and H. Sundu, Chin. Phys. C **45**, 053103 (2021).
- [43] J. He, Eur. Phys. J. C **79**, 393 (2019).
- [44] H.X. Huang, J. He and J.L. Ping, arXiv: 1904.00221 [hep-ph].
- [45] N. Yalikul, Y.H. Lin, F.K. Guo, Y. Kamiya, and B.S. Zou, Phys. Rev. D **104**, 094039 (2021).
- [46] Z.G. Wang, Int. J. Mod. Phys. A **35**, 2050003 (2020).
- [47] R. Chen, Z.F. Sun, X. Liu, and S.L. Zhu, Phys. Rev. D **100**, 011502 (2019); C.W. Xiao, J. Nieves, and E. Oset, Phys. Rev. D **100**, 014021 (2019); A.N. Semenova, V.V. Anisovich, and A.V. Sarantsev, Eur. Phys. J. A **56**, 142 (2020).
- [48] A. Ali and A.Y. Parkhomenko, Phys. Lett. B **793**, 365 (2019);
- [49] M.J. Yan, F.Z. Peng, M.S. Sánchez, and M.P. Valderrama, arXiv: 2108.05306v1 [hep-ph].
- [50] S.X. Nakamura, A. Hosaka, and Y. Yamaguchi, Phys. Rev. D **104**, L091503 (2021).
- [51] R. Chen, X. Liu, X.Q. Li and, S.L. Zhu, Phys. Rev. Lett. **115**, 132002 (2015); H.X. Chen, W. Chen, X. Liu, T.G. Steele, and S.L. Zhu, Phys. Rev. Lett. **115**, 172001 (2015); J. He, Phys. Lett. B **753**, 547 (2016); L. Roca, J. Nieves, and E. Oset, Phys. Rev. D **92**, 094003 (2015).
- [52] L. Maiani, A.D. Polosa, and V. Riquer, Phys. Lett. B **749**, 289 (2015); R.F. Lebed, Phys. Rev. D **92**, 114030 (2015); Z.G. Wang, Eur. Phys. J. C **76**, 70 (2016).
- [53] R.F. Lebed, Phys. Lett. B **749**, 454 (2015); R.L. Zhu, and C.F. Qiao, Phys. Lett. B **756**, 259 (2016).
- [54] T.J. Burns and E.S. Swanson, Phys. Rev. D **100**, 114033 (2019).
- [55] M.Z. Liu, Y.W. Pan, and L.S. Geng, Phys. Rev. D **103**, 034003 (2021).
- [56] X.H. Hu and J.L. Ping, Eur. Phys. J. C **82**, 118 (2022).
- [57] H.X. Chen, W. Chen, X. Liu, and X.H. Liu, Eur. Phys. J. C **81**, 409 (2021).
- [58] Z.G. Wang, Int. J. Mod. Phys. A **36**, 2150071 (2021).
- [59] K. Azizi, Y. Sarac, and H. Sundu, Phys. Rev. D **103**, 094033 (2021).
- [60] R. Chen, Phys. Rev. D **103**, 054007 (2021); R. Chen, Eur. Phys. J. C **81**, 122 (2021).
- [61] J.T. Zhu, L.Q. Song, and J. He, Phys. Rev. D **103**, 074007 (2021).
- [62] M.L. Du, Z.H. Guo, and J.A. Oller, Phys. Rev. D **104**, 114034 (2021).
- [63] A.N. Semenova, V.V. Anisovich, and A.V. Sarantsev, Eur. Phys. J. A **56**, 142 (2020).
- [64] K. Azizi, Y. Sarac, and H. Sundu, arXiv: 2112.15543v1 [hep-ph].
- [65] F.L. Wang, R. Chen, and X. Liu, Phys. Rev. D **103**, 034014 (2021).